Laser Ablation Synthesis of Gold Nanoparticles in Organic Solvents

Vincenzo Amendola,[†] Stefano Polizzi,[‡] and Moreno Meneghetti*[,†]

Department of Chemical Sciences, University of Padova, Via Marzolo 1, I-35131 Padova, Italy, and Department of Physical Chemistry, University of Venezia, Via Torino 155/b, I-30172 Venezia, Italy

Received: January 24, 2006; In Final Form: February 23, 2006

Free and functionalized gold nanoparticles are synthesized by laser ablation of a gold metal plate immersed in dimethyl sulfoxide, acetonitrile, and tetrahydrofuran. Functionalized gold nanoparticles are synthesized in a one-step process thanks to the solubility of the ligands in these solvents. It is possible to have significant control of the concentration, aggregation, and size of the particles by varying a few parameters. UV−vis spectroscopy and transmission electron microscopy are used for the characterization of the nanoparticles. The Mie model for spherical particles and the Gans model for spheroids allow a fast and reliable interpretation of experimental UV−vis spectra.

Introduction

Gold nanoparticles (AuNP) are interesting materials that find applications in many fields of applied and basic research. For instance, AuNPs have been used for single electron devices,[1] scanning laser microscopy in cellular mechanism studies,[2] as ultrasensible biosensors,[3] for catalysis,[4] in the synthesis of self-assembling nanomaterials,[5] and for photovoltaic devices[6] and nonlinear optics.[7]

The control of size, shape, and surface functionalization are very important issues in AuNP synthesis. Good control has been achieved with the AuNP synthesis by chemical reduction of gold ions in solution.[8] Unfortunately in this case it is difficult to remove excess reagents, such as residual surfactants or ions, or to functionalize AuNP with many kinds of molecules.[9]

A new methodology based on laser ablation in water of the bulk metal appeared in the last few years for the synthesis of gold nanoparticles.[10] Mafunè et al. have shown that it is also possible to obtain good control of the dimensions of the nanoparticles by using the second harmonic of a Nd:YAG laser (532 nm) and a surfactant like sodium dodecyl sulfate (SDS).[10] With this technique, further results have been obtained by Compagnini et al., who demonstrated the possibility of AuNP synthesis by laser ablation in solvents such as alkanes and aliphatic alcohols, as well as the possibility of obtaining the inclusion of the nanoparticles in polymer and sol−gel matrices.[11] Unfortunately, many molecules useful for functionalizing AuNPs are not soluble in these solvents. Therefore, we studied the synthesis of gold nanoparticles by laser ablation in solutions of dimethylsulfoxide (DMSO), tetrahydrofuran (THF), and acetonitrile (CH_3CN), which are solvents largely used in organic synthesis. We obtained free or functionalized AuNP in a one-step process by laser ablation of a gold plate immersed in pure solvents or in solutions of ligand molecules. This makes it possible to obtain a direct and easy functionalization of the nanoparticles without other interfering reagents and therefore to obtain a new nanostructure with new properties. For example, an enhancement of the multiphoton absorption of fullerene excited with nanosecond pulses at 532 nm was found when gold nanoparticles were coupled to a functionalized fullerene in DMSO, where this molecule was sufficiently soluble.[12] Different results were found in the synthesis of gold nanoparticles with toluene as a solvent[13] because in this case we obtained nanoparticles with small radii (about 1.0 nm) covered with graphite and without the characteristic surface plasmon absorption.

Laser ablation in solution is a simple and rapid technique and it allows some control of AuNP concentration, size, and aggregation by the variation of a few parameters. Further control of gold nanoparticle aggregation and size is achieved by laser treatment at 532 nm using their characteristic surface plasmon absorption (SPA).

Because the SPA is dependent on AuNP size and shape, UV−vis spectroscopy allowed the characterization of the colloidal solutions by fitting the spectra with the Mie model for compact spheres and the Gans model for spheroids. Transmission electron microscopy (TEM) analysis supported and complemented the conclusions obtained through the fitting of UV−vis spectra.

Experimental Section

Laser ablation was obtained with Nd:YAG (Quantel YG981E) laser pulses at 1064 nm (9 ns) focused with a 10-cm focus lens on a gold plate placed at the bottom of a cell containing the solvent or the solution. We used pulses of about 10 J cm^{-2} at a 10 Hz repetition rate for 10 min. Size reduction and reshaping of AuNPs were obtained with the second harmonic of the Nd:YAG laser at 532 nm and fluences of 1−5 J cm^{-2} at 1 Hz for 5−10 min.

All solvents were of spectroscopic grade, and the target was a plate of 99.9% pure gold.

UV−vis spectra were recorded with a Varian Cary 5 spectrometer in 2 mm optical path quartz cells.

TEM images were collected at 300 kV with a JEOL JEM 3010 microscope equipped with a Gatan Multiscan CCD Camera model 794. The samples were prepared by evaporating some gold nanocluster solution on a copper grid covered with an amorphous carbon holey film.

Model for Fitting AuNP UV−Vis Spectra. Information about the structure of AuNP can be obtained with the interpreta-

* To whom correspondence should be addressed. E-mail: moreno.meneghetti@unipd.it.
[†] University of Padova.
[‡] University of Venice.

10.1021/jp0605092 CCC: $33.50
Published on Web 03/17/2006

tion of the UV−vis spectra on the basis of the Mie theory.[14] AuNPs with nanometric sizes have a characteristic red color due to their SPA.[15] For spherical gold nanoparticles, the SPA is located near 520 nm and its frequency maximum depends mainly on the size and the refraction index of the environment.[14]

The absorption cross sections of AuNPs can be calculated using the Mie model for compact spheres. The Mie model is based on the resolution of the Maxwell equations in spherical coordinates using the multipoles expansion of the electric and magnetic fields and accounting for the discontinuity of the dielectric constant between the sphere and the surrounding medium.[14,16] When the sphere radius (R) is much smaller than the electromagnetic radiation wavelength, the multipolar expansion can be truncated to the first term (dipolar approximation). For gold the dipolar approximation is valid for $R < 20$ nm. One should also recall that for $R < 0.7$ nm the model is no more valid because below this dimension quantum size effects become relevant.[17] In the dipolar approximation the extinction cross section (σ_{ext}) is[14]

$$\sigma_{ext} = 9\frac{\omega}{c}\epsilon_m^{3/2} V \frac{\epsilon_2(\omega,R)}{[\epsilon_1(\omega,R) + 2\epsilon_m]^2 + \epsilon_2(\omega,R)^2} \quad (1)$$

where c is the light speed, ω is the radiation frequency, V is the volume of the single sphere of radius R and dielectric constant $\epsilon(\omega,R) = \epsilon_1(\omega,R) + i\epsilon_2(\omega,R)$, and ϵ_m is the host medium dielectric constant. The dielectric constant is R-dependent because it can be corrected using a size-dependent relaxation frequency $\Gamma(R)$ by the introduction of the following relationship[14]

$$\Gamma(R) = \Gamma_\infty + A\frac{v_F}{R} \quad (2)$$

where Γ_∞ is the bulk metal value, v_F is the Fermi speed, and A is a parameter that will be considered equal to 1. Therefore, $\epsilon(\omega,R)$ can be written in the following way

$$\epsilon(\omega,R) = \left\{\epsilon_{1\infty}(\omega) + \omega_P^2\left(\frac{1}{\omega^2+\Gamma_\infty^2} - \frac{1}{\omega^2+\Gamma(R)^2}\right)\right\} + i\left\{\epsilon_{2\infty}(\omega) + \frac{\omega_P^2}{\omega}\left(\frac{\Gamma(R)}{\omega^2+\Gamma(R)^2} - \frac{\Gamma_\infty}{\omega^2+\Gamma_\infty^2}\right)\right\} \quad (3)$$

where ω_P is the plasma frequency and $\epsilon_{1\infty}(\omega)$ and $\epsilon_{2\infty}(\omega)$ are real and imaginary components of bulk metal dielectric function. For bulk gold we used the dielectric constant measured by Johnson and Christy.[18]

In almost all cases we have found that the fitting of experimental UV−vis spectra with the Mie model is not adequate in the wavelength range above 600 nm, where the absorption is larger than that calculated. This finding can be explained if we consider that the Mie model accounts only for particles with spherical shape, which is usually the shape obtained by a laser ablation synthesis (see below). However, AuNPs in solution also form aggregates with nonspherical shapes, particularly when surfactants are not present, and this is the most important reason for observing deviations of the experimental spectra above 600 nm with respect to the calculated spectra with the Mie model. TEM images, although only in part representative of particle aggregation in solution, often show cigarlike shapes, which can be modeled, in a first approximation, by prolate spheroids. UV−vis spectra of spheroidal nanoparticles have two characteristic absorption bands, one at the same frequency of spherical particles due to the polarization along the shorter axes and the other due to the polarization along the longer axis, red shifted and usually more intense with respect to the first.[14] This last feature can account for the absorption above 600 nm that we observed. Therefore, we have considered that the interpretation of our spectra can also be completed including a description of the behavior of such nonspheroidal particles. For calculating the extinction cross section of spheroids randomly oriented in space we used the Gans model, which is the extension, within the dipolar approximation, of the Mie model for spheroidal shapes. For a prolate spheroid of aspect ratio a/b, where b is the smaller axis ($a > b = c$), σ_{ext} is[14,19]

$$\sigma_{ext}(\omega) = \frac{V\epsilon_m^{3/2}\omega}{3c}\sum_j \frac{\frac{1}{P_j^2}\epsilon_2}{\left(\epsilon_1 + \frac{1-P_j}{P_j}\epsilon_m\right)^2 + \epsilon_2^2} \quad (4)$$

$$P_a = \frac{1-e^2}{e^2}\left[\frac{1}{2e}\ln\left(\frac{1+e}{1-e}\right) - 1\right] \quad (5)$$

$$P_b = P_c = \frac{1-P_a}{2} \quad (6)$$

where $V = 4(\pi/3)\cdot ab^2$ is the volume and $e = [1 - (b/a)^2]^{1/2}$ is the eccentricity of the spheroid.

One can think that spheroidal particles show a distribution of aspect ratios because aggregation can involve two or more particles and we have assumed a Gaussian probability $G(a/b)$ centered at $a/b = 1$ for such a distribution

$$G(a/b) = \frac{1}{\sigma_G\sqrt{2\pi}}\exp\left[-\frac{(a/b-1)^2}{2\sigma_G^2}\right] \quad (7)$$

where $a/b > 1$ and σ_G is the standard deviation, which indicates that 68% of spheroidal particles have a/b smaller than $1 + \sigma_G$.

Samples contain nanoparticles with different radii and different levels of aggregation. However, one can try to have an average description of the nanoparticles in particular when their distribution is not very wide. Following this approach we found that the UV−vis experimental data can be reproduced by using Mie and Gans models and only three fitting parameters: (i) one average radius of the nanoparticles (R); (ii) the standard deviation (σ_G) of the a/b Gaussian distribution; and (iii) the fraction of spherical to spheroidal gold nanoparticles. Furthermore, the geometrical average of the spheroid's semiaxes was considered to be equal to the average sphere radius, that is, $R = \sqrt[3]{ab^2}$, considering, therefore, that all the particles have the same volume and avoiding the introduction of other parameters. A χ^2 fitting was used for the calculation of the spectra. Initialization of the calculation was obtained estimating the initial average radius, R, by fitting the spectral region around 520−530 nm with the Mie model, whereas the initial fraction of spheroids and their distribution was obtained by fitting the region above 600 nm using the Gans model because a small contribution is due, in this spectral region, to spherical particles smaller than 20 nm, as in our cases (see below). Scaling the values of the calculated spectra to the experimental ones allows the determination of the concentration of the nanoparticles.

We have used this type of fitting for characterizing the synthesis in different solvents and to understand the evolution

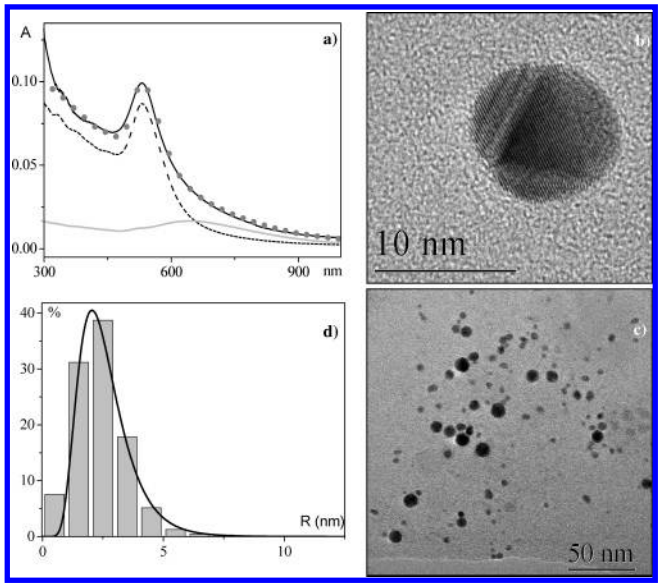

Figure 1. (a) UV−vis spectrum of AuNP synthesized in DMSO (black line), the Mie−Gans fitting (circles) [see text], the spherical particles contribution to the fitting (dashed line) and the spheroids contribution (grey line). (b−c) HRTEM images of AuNP from the same solution. (d) The nanoparticle size distribution fitted with a log−normal curve.

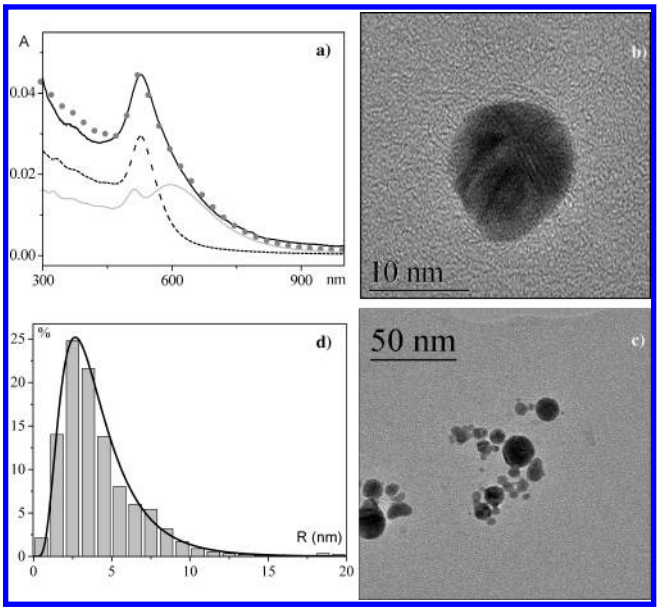

Figure 2. (a) UV−vis spectrum of AuNP synthesized in THF (black line), the Mie−Gans fitting (circles) [see text], the spherical particles contribution to the fitting (dashed line) and the spheroids contribution (grey line). (b−c) HRTEM images of AuNP from the same solution. (d) The AuNP size distribution fitted with a log−normal curve.

of the spectra with time and under laser irradiation. Comparison with TEM images has given further support to this model fitting.

Results

AuNP Laser Ablation Synthesis. Figure 1a shows the UV−vis experimental spectrum of gold nanoparticles synthesized by laser ablation in pure DMSO, where the SPA maximum is observed at 530 nm. Figure 1b and c shows representative TEM images of the same sample where particles with largely spherical shapes can be observed, as recalled above, and as expected for a laser ablation synthesis. Aggregation can also be observed but cannot be, evidently, considered representative of the situation in solution. AuNPs show clear crystalline structures, and we measured an average radius $R = 2.4$ nm with a standard deviation of 0.9 nm on 360 nanoparticles. As it is possible to see in Figure 1d, the size distribution obtained from TEM images can be fitted by a log−normal curve with a peak at 2.4 nm and a width of 0.4. The Mie−Gans fitting of the UV−vis spectrum (Figure 1a) finds an average radius of $R = 2.5$ nm, that is in very good agreement with TEM measurements. Figure 1a also shows the separate contributions of spheres and spheroids to the final fitting. Only 10% of gold nanoparticles are found to be spheroids with a Gaussian distribution of aspect ratio with a standard deviation $\sigma_G = 1.4$.

Figure 2a shows the UV−vis spectrum of AuNP synthesized in pure THF, where the SPA is centered at 528 nm. Figure 2b and c shows TEM images of the same sample. The nanoparticle average radius measured from TEM analysis is $R = 4.1$ nm with a standard deviation of 2.5 nm analyzing more than 440 particles. The particle size distribution (Figure 2d) is similar to that reported for AuNP in DMSO although with a larger width. The log−normal curve shows a peak at 3.6 nm and a width of 0.55. The Mie−Gans fitting of the UV−vis spectra (Figure 1a) indicates an average radius of $R = 4.5$ nm, which is close to the average radius measured with TEM analysis. In this case the peak of the log−normal is at lower values because of the larger width of the distribution. The spheroid's contribution is found to be 34% with $\sigma_G = 1.0$ and it is reported in Figure 2a together with the sphere's contribution.

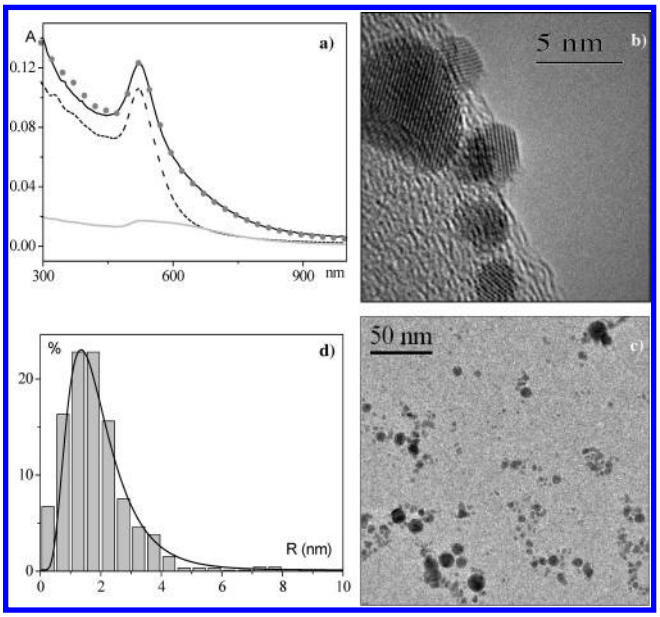

Figure 3. (a) UV−vis spectrum of AuNP synthesized in CH_3CN (black line), the Mie−Gans fitting (circles) [see text], the spherical particles contribution to the fitting (dashed line) and the spheroids contribution (grey line). (b−c) HRTEM images of AuNP from the same solution. (d) The nanoparticle size distribution fitted with a log−normal curve.

Figure 3a shows the UV−vis experimental spectrum of a AuNP synthesized by laser ablation in pure CH_3CN, in which the SPA is located at 522 nm. TEM images relative to the same sample are reported in Figure 3b and c. In this case the AuNP average radius is found to be $R = 1.8$ nm with a standard deviation of 1.2 nm observing 430 particles. The log−normal curve of the distribution of particles has a peak at 1.8 nm and a width of 0.5. The Mie−Gans fitting (Figure 3a) finds an average radius $R = 2.7$ nm with a fraction of 14% of spheroids with $\sigma_G = 1.2$.

The solutions of free nanoparticles, without any stabilizing agent, are stable at least for several hours at room temperature without any appreciable change of their UV−vis spectrum. This

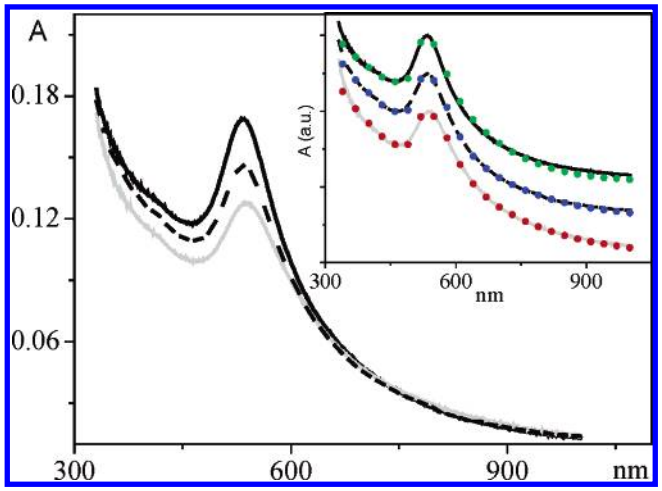

Figure 4. UV−vis spectra of AuNP in DMSO as synthesized (black line), after 5 min of size reduction at 532 nm (dashed line) and after 10 min (grey line). Inset: Mie−Gans fitting of the UV−vis spectra before the treatment (green circles), after 5 min of treatment (blue circles), and after 10 min (red circles). Curves are displaced for clarity.

allows an easy manipulation of the particles for further functionalization or for their inclusion in solid matrices such as polymers or sol−gel materials. Some relevant aggregation is observed on a time scale of days or weeks although it can be controlled by further laser treatment (see below). This situation also offers the possibility of an easy functionalization of the nanoparticles without the problem of controlling exchange equilibrium with capping agents.

Processing AuNP: Size Reduction and Reshaping. It is expected that laser treatment of AuNP allows a size reduction or reshaping of the AuNP as a function of the energy and duration of pulses.[20] For larger energies, which also depend on the duration of pulses, one can obtain a reduction of the average diameter of the particles. The interpretation of such a reduction is believed, in particular using nanosecond pulses, to be due to photothermal effects.[20] One finds that larger particles are reduced as a consequence of their increased temperature to the boiling point, or, if such a temperature is not reached, to a temperature that allows the formation of a layer of vapor on the surface of the nanoparticles.[20b] Clearly, such a behavior can be observed when the dissipation of energy is not sufficient and therefore the temperature can increase, and this also depends on the surrounding of the molecules and if they are capped or not. However, also not considering the details, one expects that smaller particles show time constants of heat dissipation that are proportional to the square of their radius.[20b] Smaller nanoparticles show, therefore, fast heat dissipation and they are less expected to reach a temperature sufficient for reduction. This explains, therefore, the observation that larger particles are reduced to smaller particles. We obtained results that agree with such a prediction.

As an example, Figure 4 shows the UV−vis spectra of AuNP solution in DMSO as synthesized, after 5 min of size reduction at 532 nm (4 J/cm^2 at 1 Hz) and after 10 min. The Mie−Gans fitting (inset of Figure 4) indicates that the average size goes from 2.5 to 1.8 nm after 5 min and to 1.5 nm after 10 min. The presence of spheroids goes from 21% ($\sigma_G = 1.0$) after the synthesis to 9% ($\sigma_G = 1.4$) after 5 min of treatment to 11% ($\sigma_G = 1.4$) after 10 min. Therefore, the aggregation also decreases after the size reduction. The resulting solutions are stable for several days without any capping agent.

When the laser fluence is not high enough, AuNPs do not absorb the energy required by size reduction. However, this process usually leads to the reshaping of AuNPs with edges or spheroidal forms into spheres.[19,20b,21] Also in our case we observe some changes of the UV−vis spectra, but because most of the particles are already spheres we interpret the variation as due to a different aggregation of the particles, which is the main source of nonspherical forms of our particles.

To show this effect, Figure 5a reports the UV−vis spectra of a solution of AuNPs in THF before and after treatment at 532 nm with a fluence of 1 J/cm^2 for 5 min at 1 Hz. The Mie−Gans fitting of the UV−vis spectra (Figure 5b) indicates that the as synthesized solution has a 76.5% fraction of spheroidal particles (average radius $R = 9.0$ nm and $\sigma_G = 0.9$), whereas after treatment there are only 22% of spheroids ($R = 10.0$ nm and $\sigma_G = 1.0$). Therefore, one finds that the aggregation is reduced strongly after the laser treatment at low energy. However, the process is fully reversible. In fact, after 1 day the aggregation again increases the spheroid fraction to 59% ($R = 9.0$ nm and $\sigma_G = 1.0$), but irradiating the solution at 532 nm (5 min, 1 Hz and 1 J/cm^2) the fraction of spheroidal particles is again reduced to 22% ($R = 10.0$ nm and $\sigma_G = 1.0$).

These results represent a simple way to control AuNP size or aggregation without other interfering molecules absorbed on their surface.

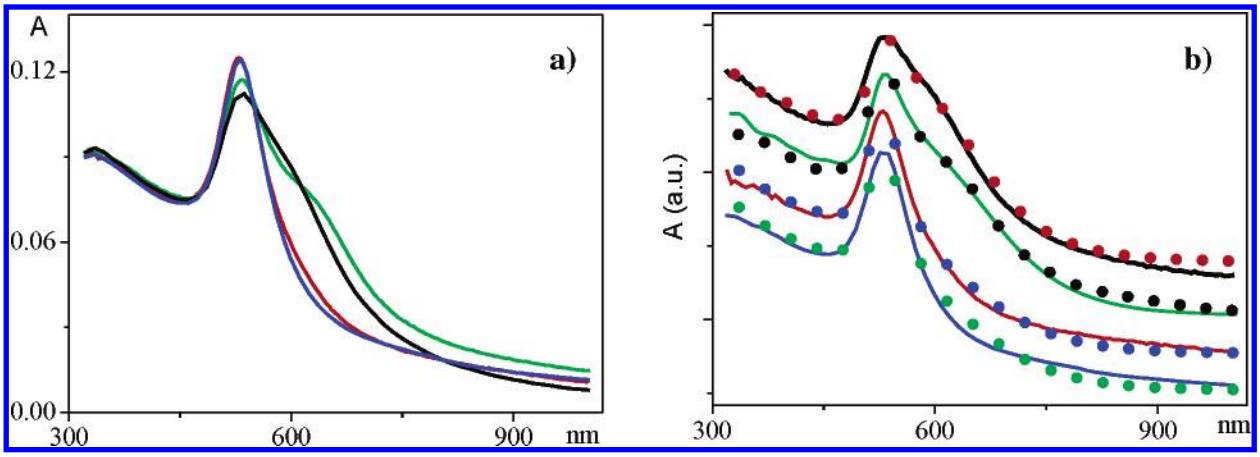

Figure 5. (a) UV−vis spectra of AuNP in THF as synthesized (black line), after reshaping at 532 nm (red line), after 24 h (green line), and after the second reshaping treatment (blue line). (b) Mie−Gans fitting of the as synthesized solution (experimental: black line, fitting: red circles), of the treated solution (experimental: red line, fitting: blue circles), of the solution after 24 hours (experimental: green line, fitting: black circles) and after the last reshaping (experimental: blue line, fitting: green circles). Curves are vertically displaced for clarity.

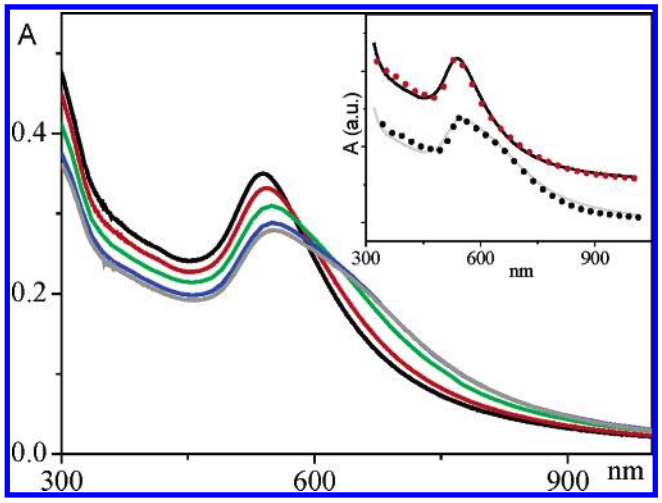

Figure 6. UV−vis spectra of AuNP in DMSO as synthesized (black line), after 2 h (grey line), after 1 day (green line), after 5 days (blue line), and after 6 days (red line). Inset: Mie−Gans fitting of the as synthesized solution (experimental: black line, fitting: red circles) and of the 6-days-aged solution (experimental: grey line, fitting: black circles). Curves are vertically displaced for clarity.

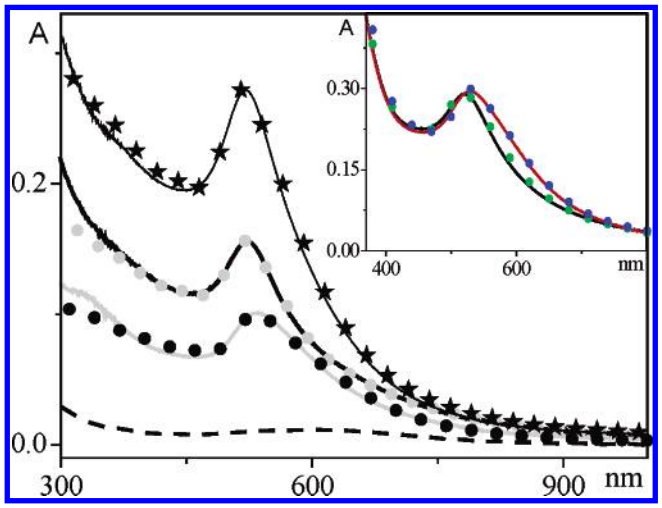

Figure 7. UV−vis spectrum of AuNP as synthesized in CH_3CN with 5.2×10^{13} AuNP/cm^3 concentration (thin black line), the Mie−Gans fitting (black stars), the UV−vis spectrum of the same solution after 20 h (dashed line) with almost all particles precipitated. The spectrum of a 3.8×10^{13} AuNP/cm^3 solution as synthesized (thick black line), the Mie−Gans fitting (grey circles), and the spectrum of the same solution after 2 weeks (grey line) with the Mie−Gans fitting (black circles). Inset: UV−vis spectra of 1.3×10^{14} AuNP/cm^3 as synthesized in a 10^{-2} M solution of AT in CH_3CN (black line), of the same solution after 20 h (red line), the Mie−Gans fitting for the AuNP as synthesized in AT + CH_3CN (green circles) and after 20 h (blue circles).

Aging of AuNP Solutions. Aging of the solution of free nanoparticles leads to large aggregation in particular because they are not capped with other molecules that could induce electrostatic repulsion between the particles, if they are charged, or to steric effects like in the case of polymers.[20a]

Figure 6 shows the aging effect on the UV−vis spectra of AuNP in DMSO. The Mie−Gans fitting (inset of Figure 6) indicates that the as synthesized solution has 25% of spheroidal nanoparticles with $\sigma_G = 0.9$ and average radius $R = 2.5$ nm, while the same solution after 6 days has 100% of spheroidal particles with $\sigma_G = 1.0$ and average radius $R = 4.0$ nm. Similar situations were found with the other solvents.

The aggregation of the AuNP solutions can be controlled without any capping molecule by simply reducing the concentration of the AuNP. For example, Figure 7a shows that the dynamics of aggregation of an AuNP solution in CH_3CN, which at last determines the precipitation of the particles, changes as a consequence of a variation of the particle concentration. We evaluated, by a Mie−Gans fitting, that the concentration of the solution that showed a large precipitation after 20 h was 5.2×10^{13} AuNP/cm^3 ($R = 2.5$ nm, 29% of spheroids with $\sigma_G = 0.8$) and that of a solution with a larger stability (more then 2 weeks before significant precipitation) 3.8×10^{13} AuNP/cm^3 ($R = 2.5$ nm, 12% of spheroids with $\sigma_G = 1.2$). Further experiments are needed to understand the concentration dependence of the dynamics of aggregation. However, as expected, one can control the process of aggregation and the following precipitation by adding a ligand molecule, for example, thioctic acid (AT: $C_8H_{14}O_2S_2$) at a concentration of 10^{-2} M. AT has a disulfide group able to form two chemical S−Au bonds on the AuNP surface. The inset of Figure 7 shows that the synthesis of AuNP in a solution of thioctic acid slows down aggregation and precipitation. In this case the Mie−Gans fitting of the as synthesized AuNP indicates a concentration of 1.3×10^{14} AuNP/cm^3, larger with respect to the above cases, an average radius $R = 2.0$ nm and a 19% fraction of spheroids with $\sigma_G = 0.8$. After 20 h one finds that the UV−vis spectrum changes are only due to some initial aggregation. In fact, the fitting indicates that there are 51% of spheroids with $\sigma_G = 0.8$ and an average radius of $R = 2.5$ nm.

Conclusions

We have shown how it is possible to obtain, in a time scale of minutes, stable and free AuNPs in organic solvents such as DMSO, THF, and CH_3CN by a simple laser ablation methodology. The solutions were found to be stable for hours to weeks, and the size and aggregation of the AuNPs were controlled by laser irradiation. Fitting of the UV−vis spectra with a Mie−Gans model allowed us to have a description of the average characteristics of the AuNP, which compare well with TEM measurements. The fitting of the UV−vis spectra was found, therefore, to be a useful and reliable characterization of the AuNP.

Acknowledgment. We thank G. Marcolongo and S. Crivellaro for technical help. MIUR is gratefully acknowledged for financial support (FIRB/RBNE033KMA, FIRB/RBNE01P4JF and PRIN2004/200035502).

References and Notes

(1) (a) Feldheim, D. L.; Keating, C. D. *Chem. Soc. Rev.* **1998**, *27*, 1−12. (b) Gittins, D. I.; Bethell, D.; Schiffrin, D. J.; Nichols, R. J. *Nature* **2000**, *408*, 67−69.

(2) (a) Boyer, D.; Tamarat, P.; Maali, A.; Lounis, B.; Orrit, M. *Science* **2002**, *297*, 1160−1163. (b) Yelin, D.; Oron, D.; Thiberge, S.; Moses, E.; Silberberg, Y. *Opt. Express* **2003**, *11*, 1385−1391.

(3) (a) Schneider, B. H.; Dickinson, E. L.; Vach, M. D.; Hoijer, J. V.; Howard, L. V. *Biosens. Bioelectron.* **2000**, *15*, 597−604. (b) Nam, J. M.; Thaxton, C. S.; Mirkin, C. A. *Science* **2003**, *301*, 1884−1886.

(4) (a) Henglein, A. *J. Phys. Chem.* **1993**, *97*, 5457−5471. (b) Kamat, P. V. *J. Phys. Chem. B* **2002**, *106*, 7729−7744.

(5) Jackson, A. M.; Myerson, J. W.; Stellacci, F. *Nat. Mater.* **2004**, *3*, 330−336.

(6) Sudeep, P. K.; Ipe, B. I.; Thomas, K. G.; George, M. V.; Barazzouk, S.; Hotchandani, S.; Kamat, P. V. *Nano Lett.* **2002**, *2*, 29−35.

(7) (a) Qu, S.; Du, D.; Song, Y.; Wang, Y.; Gao, Y.; Liu, S.; Li, Y.; Zhu, D. *Chem. Phys. Lett.* **2002**, *365*, 403−408. (b) Qu, S.; Song, Y.; Du, C.; Wang, Y.; Gao, Y.; Liu, S.; Li, Y.; Zhu, D. *Chem. Phys. Lett.* **2001**, *196*, 317−323.

(8) (a) Yonezawa, T.; Kunitake, T. *Colloids Surf., A* **1999**, *149*, 193−199. (b) Watson, K. J.; Zhu, J.; Nguyen, S. B. T.; Mirkin, C. A. *J. Am. Chem. Soc.* **1999**, *121*, 462−463. (c) Brust, M.; Walker, M.; Bethell, D.; Schiffrin, D. J.; Whyman, R. J. *J. Chem. Soc., Chem. Commun.* **1994**, 801−

802. (d) Brust, M.; Fink, J.; Bethell, D.; Schiffrin, D. J.; Kiely, C. J. *J. Chem. Soc., Chem. Commun.* **1995**, 1655−1656. (e) Jana, N. R.; Gearheart, L.; Murphy, C. J. *J. Phys. Chem. B* **2001**, *105*, 4065−4067.

(9) Prochazka, M.; Stepanek, J.; Vlckova, B.; Srnova, I.; Maly, P. *J. Mol. Struct.* **1997**, *410*, 213−216.

(10) (a) Mafune, F.; Kohno, J.; Takeda, Y.; Kondow, T.; Sawabe, H. *J. Phys. Chem. B* **2001**, *105*, 5114−5120. (b) Mafune, F.; Kohno, J.; Takeda, Y.; Kondow, T. *J. Phys. Chem. B* **2001**, *105*, 9050−9056. (c) Mafune, F.; Kohno, J. Y.; Takeda, Y.; Kondow, T. *J. Phys. Chem. B* **2002**, *106*, 8555−8561. (d) Mafune, F.; Kohno, J. Y.; Takeda, Y.; Kondow, T. *J. Phys. Chem. B* **2002**, *106*, 7575−7577. (e) Mafune, F.; Kohno, J. Y.; Takeda, Y.; Kondow, T. *J. Phys. Chem. B* **2003**, *107*, 4218−4223. (f) Mafune, F.; Kondow, T. *Chem. Phys. Lett.* **2003**, *372*, 199−204.

(11) (a) Compagnini, G.; Scalisi, A. A.; Puglisi, O.; Spinella, C. *J. Mater. Res.* **2004**, *19*, 2795−2798. (b) Compagnini, G.; Scalisi, A. A.; Puglisi, O. *J. Appl. Phys.* **2003**, *94*, 7874−7877.

(12) Amendola, V.; Mattei, G.; Cusan, C.; Prato, M.; Meneghetti, M. *Synth. Met.* **2005**, *155*, 283−286.

(13) Amendola, V.; Rizzi, G. A.; Polizzi, S.; Meneghetti, M. *J. Phys. Chem. B* **2005**, *109*, 23125−23128.

(14) (a) Kreibig, U.; Vollmer, M. *Optical Properties of Metal Clusters*; Springer-Verlag: Berlin, 1995. (b) Bohren, C. F.; Huffman, D. R. *Absorption and Scattering of Light by Small Particles*; Wiley: New York, 1983. (c) Link, S.; El-Sayed, M. *J. Phys. Chem. B* **1999**, *103*, 8410−8426.

(15) Daniel, M. C.; Astruc, D. *Chem. Rev.* **2004**, *104*, 293−346.

(16) (a) Mie, G. *Ann. Phys.* **1908**, *25*, 377. (b) Stratton, J. A. *Electromagnetic Theory*; McGraw-Hill: New York, 1941.

(17) Alvarez, M. M.; Khoury, J. T.; Schaaff, T. G.; Shafigullin, M. N.; Vezmar, I.; Whetten, R. *J. Phys. Chem. B* **1997**, *101*, 3706−3712.

(18) Johnson, P. B.; Christy, R. W. *Phys. Rev. B* **1972**, *6*, 4370−4379.

(19) Link, S.; El-Sayed, M. A. *J. Phys. Chem. B* **1999**, *103*, 8410−8426.

(20) (a) Link, S.; El-Sayed, M. A. *Rev. Phys. Chem.* **2000**, *19*, 409−453. (b) Inasawa, S.; Sugiyama, M.; Yamaguchi, Y. *J. Phys. Chem. B* **2005**, *109*, 9404−9410. (c) Inasawa, S.; Sugiyama, M.; Yamaguchi, Y. *J. Phys. Chem. B* **2005**, *109*, 3104−3111. (d) Kabashin, A. V.; Meunier, M. *J. Appl. Phys.* **2003**, *94*, 7941−7943.

(21) (a) Link, S.; Burda, C.; Mohamed, M. B.; Nikoobakht, B.; El-Sayed, M. A. *J. Phys. Chem. B* **1999**, *103*, 1165−1170. (b) Link, S.; Burda, C.; Nikoobakht, B.; El-Sayed, M. A. *J. Phys. Chem. B* **2000**, *104*, 6152−6163.